The role of feedstock and activation process on supercapacitor performance of lignocellulosic biochar

Biomass and Bioenergy 184 (2024) 107180

Contents lists available at ScienceDirect

Biomass and Bioenergy

journal homepage: www.elsevier.com/locate/biombioe

The role of feedstock and activation process on supercapacitor performance of lignocellulosic biochar

Jiacheng Sun [a,**], Anjali Jayakumar [a,b], Carlos G. Díaz-Maroto [c], Inés Moreno [c,d], Javier Fermoso [c], Ondřej Mašek [a,*]

[a] UK Biochar Research Centre, School of Geosciences, University of Edinburgh, Crew Building, Alexander Crum Brown Road, Edinburgh, EH9 3FF, UK
[b] School of Engineering, Merz Court, Newcastle University, Newcastle Upon Tyne, NE17RU, UK
[c] Thermochemical Processes Unit, IMDEA Energy Institute, Avda. Ramón de La Sagra, 3, Móstoles, 28935, Madrid, Spain
[d] Chemical and Environmental Engineering Group, Rey Juan Carlos University, C/ Tulipán, s/n, Móstoles, Madrid, 28933, Spain

ARTICLE INFO

Keywords:
Biochar
Activation
Supercapacitor
Conductivity

ABSTRACT

Porous carbons derived from lignocellulosic biomass and their use in electrochemical applications are attracting a growing level of interest due to the sustainable nature of the materials and its favourable properties. This study investigates the influence of feedstocks and three activation methods (CO_2, steam, and KOH) on the electrochemical properties of lignocellulosic biochars. The results showed that activated biochars derived from straw biomass had a higher specific capacitance than wood-derived activated biochars, despite lower electrical conductivity and porosity. Furthermore, chemical activation using KOH was found to increase the capacitance of activated biochars compared to physical activation using steam and CO_2, although sometimes at the expense of electrical conductivity. The study highlights the importance of carefully selecting the feedstocks and activation methods to optimise the electrochemical properties of biochar for potential use as a sustainable supercapacitor material.

1. Introduction

Electrochemical energy storage devices have become increasingly important due to the global shift towards renewable energy sources [1]. According to the International Energy Agency, renewable energy sources accounted for 90% of global electricity net additions in 2021 and this trend is expected to continue [2]. As many renewable sources, such as solar and wind, are inherently unpredictable in terms of energy output, efficient energy storage technologies are crucial to tap into this renewable energy source. The global energy storage market is set to grow exponentially over the next decade, with annual installations increasing almost tenfold between 2020 and 2030 and global energy storage capacity could increase from around 14 GW in 2020 to 420 GW by 2030 [3]. Electrochemical energy storage devices, such as batteries and supercapacitors, have become popular due to their ability to store energy and release it when needed; however, the search for sustainable and efficient electrode materials is still ongoing to make these devices more efficient and environmentally friendly [4].

Supercapacitors are highly attractive for their ability to rapidly store and release energy, making them ideal for applications requiring high peak power such as electric vehicles, wind turbines, and data storage centres [5]. There are two types of supercapacitors – electrochemical double layer capacitors (EDLCs) and pseudocapacitors, which differ in their energy storage mechanisms. EDLCs store energy via electrolyte ion accumulation at the nanomaterial interface electrostatically, whereas pseudocapacitors involve faradaic redox reactions on electrode/electrolyte interface, which only have electron-transfer without chemical reactions [1]. Carbon materials such as graphite [4], activated carbon [6], graphene [7], carbon nanotubes [8], and carbon aerogels [9] have been widely used as supercapacitor electrode materials, but they have limitations such as being unsustainable, costly, and having a high carbon footprint [10]. Biochar, is a carbonaceous solid product of biomass pyrolysis, recognised as a carbon-negative technology due to its ability to sequester carbon in different applications for hundreds to thousands of years, thereby effectively removing CO_2 from the atmosphere [11–14]. However, raw biochar has a relatively low surface area

* Corresponding author.
** Corresponding author.
E-mail addresses: jiacheng.sun@hotmail.com (J. Sun), ondrej.masek@ed.ac.uk (O. Mašek).

https://doi.org/10.1016/j.biombioe.2024.107180
Received 31 January 2024; Received in revised form 20 March 2024; Accepted 20 March 2024
Available online 23 March 2024

(10–100 $m^2\ g^{-1}$) and requires additional post-treatments such as activation, surface heteroatom doping, and making composites with metal oxides/hydroxides to improve its electrochemical properties [1]. An activation step to improve the properties of biochar could most often be achieved in the same unit that is used to produce the biochar, making it a practical post-treatment step for biochar and its subsequent use for electrochemical applications, with minimal requirement for additional processing steps.

Commercial activated carbons produced from coal or coke-have a negative environmental impact, with carbon footprint of 8.34 kg CO_2eq kg^{-1} and cost of 1.34 $ kg^{-1} [15]. Therefore, biomass-derived alternatives offer a better prospect. Activation technologies can be classified as physical or chemical depending on the reactions that occur during the processing. Physical activation involves the use of steam, carbon dioxide, and other reactive gases, typically at temperatures between 700 and 900 °C, causing the biochar to auto-gasify and leading to the formation of more porous solid products through the loss of mass [16]. For example, Yang et al. synthesised a biochar electrode from resin with CO_2 activation at 600–1000 °C, resulting in a surface area of 2991.1 $m^2\ g^{-1}$, pore size of 2.4 nm, micropore volume of 1.33 $cm^3\ g^{-1}$, and total pore volume of 1.81 $cm^3\ g^{-1}$ [17]. Physical carbon activation occurs mostly through the non-selective removal of carbon from the carbon material surface, whereas, chemical activation causes a number of reactions that remove non-graphitic components from the carbon particles in a selective way [17]. Zhao et al. employed KOH as an agent to activate corncobs at temperature of 600–750 °C, producing a high surface area material (2998 $m^2\ g^{-1}$) with a large micropore/mesopore ratio (8.26) that demonstrated promising pore-tuning effects [18]. The resulting biomass-based activated carbon could be more sustainable in comparison with coal-based activated carbon electrodes, while achieving comparable performance, making it a potential candidate for use as a greener supercapacitor electrode material [15].

To improve the performance of supercapacitor electrodes using activation methods, it is essential to enhance their specific surface area and electrical conductivity (EC) among other properties [5,9]. Although nanostructure can increase the former, it often results in elevated electrical resistance due to the increased number of contact points. For example, when subjected to high pressure (5 MPa), graphene, nanotubes, and carbon black exhibit lower EC values (10^2 S/m) compared to graphite (10^3 S/m) [19]. In the case of these nano-carbons, the behaviour of EC during compaction is governed by mechanical particle arrangement and deformation mechanisms. This results in an increased contact resistance due to numerous gaps between nanoparticles. On the other hand, the EC of carbon-based electrodes can improved by integrating oxides [5] and metals [20] or tuning their amorphous/graphitic structure. For instance, Liu et al. (2016) found that MnO_2/Activated carbon composite electrode presents a superior electrical resistance of 2.92 Ω resulting in electrosorption capacity of 9.3 mg g^{-1}, which is approximately 1.6-times higher than that of the pure activated carbon electrode (5.7 mg g^{-1}) [21]. Similarly, enhanced graphitic structure was observed in cotton gin biochar via increased temperature from 300 to 750 °C, and its EC reached up to 1971 μS cm^{-1} [22]. Ideally, an electrode material should possess both high EC and high specific surface area, as achieved by some advanced materials like graphene-based materials and metal-organic frameworks [7]. However, these materials often come at a high cost and environmental impact [15]. Therefore, developing low-cost and nature-derived electrode material with electrochemical performance that can make it viable for large-scale applications is critical. Biochar is a promising candidate owing to its sustainable nature, however, the activated biochar production can be feedstock-dependant and needs extensive improvement in electrochemical performance to become a competitive alternative to existing electrode materials [1]. Therefore, choosing optimal feedstock for specific application, improving its specific capacitance, cyclic retention, energy density, and power density are essential properties to achieve this goal. One example of a successful commercial activated carbon material is natural graphite, which initially has a relatively low specific surface area of around 10 $m^2\ g^{-1}$. However, this can be increased to 500 $m^2\ g^{-1}$ through post-treatments, resulting in an average area-normalized capacitance of approximately 15 F cm^{-2} [23].

While there has been quite a lot of research on producing activated biochar for electrochemical energy storage, there has been no systematic investigation into the effect of different activation treatments on related biochar properties. This study explores the use of various chemical and physical activation methods on biochar derived from lignocellulosic biomass as a precursor for supercapacitor electrodes. This approach offers three key advantages: (1) utilising lignocellulosic waste as a precursor promotes sustainability and environmental-friendliness, with the CO_2, steam, and KOH activation processes avoiding the use of organic solvents to protect human health and the ecosystem; (2) the study investigates the impact of different biomass sources on the electrochemical performance of the resulting electrodes; and (3) unlike methods using surface heteroatom doping, metal oxides/hydroxides loading, and nanostructure compositing, the thermal activation process used in this study significantly reduces costs and simplifies the process using existing biochar production equipment such as pyrolysis.

2. Materials and methods

2.1. Biochar production

Softwood pellet (SWP), Oak (OAK), Oilseed rape straw (OSR), Miscanthus straw pellet (MSP), and Wheat straw pellets (WSP), were pyrolysed using UKBRC Stage III Unit (rotary kiln pyrolyser, UK Biochar Research Centre, Edinburgh) at temperature of 700 °C, heating rate of 79–103 °C min^{-1}, and residence time of 12–15 min. The detail apparatus setting and operating conditions can be found in the previous studies [24,25]. The biochars were labelled as XT, with X denoting the type of biomass used (SWP, OAK, OSR, MSP, and WSP) and T representing the maximum pyrolysis temperature. For instance, the softwood pellet that underwent pyrolysis at 700 °C was labelled as SWP700.

2.2. Physical and chemical activation of biochar

The activation setup consists of a stainless-steel downdraft fixed-bed reactor (30 cm diameter and 50 cm high) heated by an electrical furnace. The schematic diagram and detailed description can be found in recent previous works [26,27]. For the physical activation experiments, around 12 g of biochar (particle size between 0.4 and 2 mm) were initially loaded in the reactor inertised by an Ar flow at a rate of 0.1 L min^{-1}. Afterwards, the reactor was heated at 10 °C min^{-1} up to the activation temperature (800–900 °C). Once the sample temperature was steady, the reactor atmosphere was switched to that used for the activation. For CO_2 activation, a flow rate of 0.1 L min^{-1} CO_2 was used for 90 min at temperatures of 800 and 900 °C. Whilst for steam activation at 900 °C, 15 mg h^{-1} of Milli-Q water was continuously fed to the reactor with a syringe pump to produce steam by evaporation for 60 min, which was carried by a flow rate of 0.05 L min^{-1} of Ar.

For the chemical activation, the biochar was mixed with KOH (1:1 g/g) and 50 mL of Milli-Q H_2O and dried overnight at 100 °C in an oven. The obtained solid was placed in the activation lab-scale reactor and heated at 10 °C min^{-1} up to 700 °C in 0.1 L min^{-1} Ar and held for 60 min. Finally, to remove K^+ ions from the resulting activated biochar, it was subjected to several washes with an HCl solution (0.1 M) and Milli-Q H_2O until pH = 7. Then, the activated carbon was dried in an oven at 105 °C until constant weight.

The obtained activated biochars were then stored in centrifuge tubes for further analysis and labelled as B-AM-T, where B refers to name of the pristine biochar; AM refers to activation method, either CO_2, H_2O, or KOH; and T refers to activation temperature, either 800, or 900 °C. For instance, the softwood pellet that underwent pyrolysis at 700 °C and CO_2 activation at 900 °C was designated as SWP700–CO_2-900. As steam

and KOH activation used constant activation temperature at 900 and 700 °C, respectively, the activation temperature label was ignored, i.e., SWP700–H_2O and SWP700–KOH.

2.3. Characterisation of biochar

Proximate analysis of biochars and activated biochars were performed according to European standards. Thus, moisture content (UNE-EN ISO 18134–1:2016) was obtained heating the sample in an oven at 105 °C and kept overnight. Volatile matter (VM) content (UNE-EN ISO 18123:2016) was assessed by thermogravimetric analysis (TGA) in a thermobalance NETZSCH STA 449 heating up the sample to 900 °C at 10 °C/min and maintaining this temperature for 30 min under inert atmosphere. Ash content (UNE-EN ISO 18122:2016) was determined by combustion in a muffle furnace at 900 °C for 1 h in air atmosphere. Finally, the fixed carbon (FC) was calculated by difference. Ultimate analysis of carbonaceous samples was measured in a Thermo Scientific FLASH 2000 CHNS/O micro-elemental analyser, where C, H and N concentrations were obtained, while O concentration was calculated by difference.

Textural properties of the activated biochars were measured by N_2 and CO_2 adsorption-desorption isotherms at 77 K and 273 K, respectively, in a Micromeritics 3 Flex analyser equipped with a high-vacuum system and three 0.1 Torr pressure transducers with 60 points and equilibrium time of 60 min. Before the adsorption analysis, the samples were degassed at 140 °C for 16 h. The textural properties (specific surface area, total pore volume, and micropore surface and volume) were calculated from N_2 isotherms. Thus, the total pore volume was determined at a relative pressure of 0.97. The specific surface area was calculated by applying the Brunauer-Emmet-Teller (BET) equation. The contribution of micropores to the total volume and surface area (V_{MIC} and S_{MIC}), as well as the external surface area (S_{EXT}, including both mesopores and macropores), was estimated using the *t*-plot method. The pore size distribution (PSD) was determined through the combination of CO_2–N_2 isotherms using the SAIEUS software and applying the 2D-NLDFT model, considering slit pore geometry, as successfully tested for activated carbons.

Electrical conductivity measurements were performed using a 4-terminal milliohm meter. For each biochar, 1 g of biochar sample was in the sample chamber with cross section of 78.54 mm^2. Resistance measurements were taken using copper electrodes in a press provided by hydraulic car jack (maximum 2000 kg). To exclude the influence of bulk density, the measurement started from the first contact, and conductivity was gradually measured from 0.16 MPa to 33.12 MPa until the results stabilized.

The surface functionality of the biochar was assessed using a Fourier transform infrared spectroscopy (FTIR) spectrometer in the wavelength range of 500–4000 cm^{-1}. The crystalline structures and graphitisation degrees were identified using a micro-Raman tester (Renishaw inVia) with a green laser of wavelength 514 nm and a source energy of 20 mW at an intensity of 1%. Two areas were analysed for each sample, and averaged.

2.4. Electrochemical measurements

Working electrodes were prepared by mixing biochar and binder poly (vinylidenedifluoride) (PVDF) (Thermo Scientific, UK, regent grade) in a mass ratio of 8:1 for 5 min in a pot. Then 150 μL 1-Methyl-2-pyrrolidinone (NMP) (Sigma-Aldrich, UK, regent grade) was dropped and mixed for 10 min to form slurry/ink (homogeneous mixture). The obtained ink dispersion was sonicated for 1 h, and then drop and spread on a nickel foam (5 × 5 mm, which served as current collector) and placed in an oven to dry at 170 °C overnight. In this study, to make current collector easy to attach to the apparatus, a stainless-steel stick was attached to nickel foam, which would not affect the specific capacitance. The mass of the deposited active material was in the range of 2–3 mg.

For electrochemical measurements, a Platinum (Pt) sheet (0.5cm × 0.5 cm) and Ag/AgCl were used as the counter and reference electrode, respectively. Cyclic voltammetry (CV), galvanostatic charge/discharge (GCD), and electrochemical impedance spectroscopy (EIS) measurements were carried out on an Autolab PGSTAT101 in a temperature-controlled room with an average room temperature of 20 °C. The experiments were performed using 4 mol L^{-1} KOH as electrolyte. The CV tests were performed in the potential range of −1 to 0 V at various scan rates of 10–80 mV s^{-1}. GCD curves were recorded in the potential range of −1 to 0 V and EIS measurements were conducted at the frequency range from 0.01 to 100 kHz. The specific capacitance was calculated using the following equation:

$$C = \frac{I\Delta t}{m\Delta v} \tag{2}$$

where in equation (2), C (F g^{-1}) represents the specific capacitance; I (A) is the discharge current; Δt (s) is the discharge time; m (g) is the mass of the active material on the working electrode; and Δv (V) represents the potential window.

3. Results and discussion

3.1. Physicochemical properties of activated biochar

3.1.1. Proximate analysis and elemental analysis

Table 1 presents the results of proximate and ultimate analyses of biochar and activated carbons, showing that physical activation by CO_2 and steam significantly affects the composition of biochar by removing VM and leaving only FC and ash. In this case, wood biochar (WB) with low ash content (i.e., SWP and OAK) have a high FC content up to 97.20–98.50 wt% after physical activation, while straw biochar (SB), which include OSR, MSP, and WSP have a considerably different composition, with FC and ash contents ranging from 67.20 to 75.33 wt% and 21.00–32.80 wt%, respectively. Generally, a high ash content in biochar can increase its electrical resistance and limit its electrochemical performance by blocking the pores of the biochar, thus decreasing the effective surface area available for electrochemical reactions. For instance, Zhang et al. (2021) found that higher ash content can lead to reduced specific surface area (29.35–52.60 m^2 g^{-1}), compared to low-ash biochars with specific surface area of 55.61 m^2 g^{-1}, as the ash tends to clog the pores of the biochar, ultimately impairing its electrochemical performance [28]. However, this effect is strongly dependant on the ash composition, as some minerals, such as Fe_2O_3 and MnO_2, present in the ash can increase the pseudocapacitance of the biochar material [29]. Additionally, biochar with a low ash content and fine porosity may not necessarily lead to better electrochemical performance, as it also depends on other factors such as the presence of functional groups (e.g., N and.

S groups) that can enhance the surface chemistry of the biochar. Therefore, in the later sections, this study aims to examine the complex relationship between biomass type (low/high ash) and electrochemical performance, with a particular emphasis on the impact of ash on the pseudocapacitance of the biochar. The utilisation of KOH for chemical activation has led to a significant alteration in the chemical composition of the resulting activated biochar. In particular, the content of VM has considerably increased. This phenomenon can be attributed to the lower activation temperature, which has enabled a greater retention of VM within the biochar. This in turn affected the biochar particle structure, such as the pore formation and distribution [30], which will be discussed in Section 3.1.2.

In addition to proximate analysis, elemental composition can also affect the electrochemical performance of biochar. Due to the ash content being different among all types of biochar, the elemental composition data is presented on a dry ash-free basis (Table 1). The ultimate

Table 1
Proximate analysis (dry basis) and ultimate analysis (dry and ash free basis) for pristine and activated biochars.

Biomass type	Activation method	Sample	Proximate analysis, db (wt.%)				Elemental analysis, daf (wt.%)				H/C	O/C
			Moist.	Ash	FC	VM	C	H	N	O[a]		
Woody	N/A	SWP700	1.00	1.60	87.50	9.90	93.35	1.79	0.70	4.17	0.23	0.03
	Physical	SWP700–CO_2-800	–	1.90	98.10	–	96.20	0.30	0.40	3.10	0.04	0.02
		SWP700–CO_2-900	–	2.80	97.20	–	96.80	0.40	0.50	2.30	0.05	0.02
		SWP700–H_2O	–	2.35	97.65	–	94.42	0.65	0.09	4.85	0.08	0.04
	Chemical	SWP700–KOH	–	3.21	79.98	16.81	96.85	0.43	0.43	2.30	0.05	0.02
	N/A	OAK550	1.46	1.00	83.71	13.83	91.16	2.25	0.13	6.46	0.30	0.05
	Physical	OAK550-CO_2-800	–	2.10	97.90	–	95.90	0.50	0.30	3.30	0.06	0.03
		OAK550-CO_2-900	–	1.60	98.40	–	95.60	0.50	0.20	3.70	0.06	0.03
		OAK550-H_2O	–	1.50	98.50	–	95.62	0.48	0.59	3.32	0.06	0.03
	Chemical	OAK550-KOH	–	1.52	90.68	7.80	95.46	0.47	0.49	3.58	0.06	0.03
Straw	N/A	OSR700	2.19	21.00	63.40	13.40	90.76	1.87	0.89	6.48	0.25	0.05
	Physical	OSR700-CO_2-800	–	26.70	73.30	–	88.30	1.10	1.40	9.20	0.15	0.08
		OSR700-CO_2-900	–	32.80	67.20	–	91.77	0.88	1.35	6.00	0.12	0.05
		OSR700-H_2O	–	31.10	68.90	–	90.20	0.70	0.10	9.00	0.09	0.07
	Chemical	OSR700-KOH	–	17.26	67.56	15.18	92.96	0.85	0.73	5.46	0.11	0.04
	N/A	MSP700	1.53	18.8	69.98	9.69	89.82	1.83	1.59	6.75	0.24	0.06
	Physical	MSP700-CO_2-800	–	24.67	75.33	–	89.60	0.70	0.30	9.40	0.09	0.08
		MSP700-CO_2-900	–	28.73	71.27	–	95.30	0.70	0.50	3.50	0.09	0.03
		MSP700-H_2O	–	28.60	71.40	–	92.21	0.71	1.26	5.81	0.09	0.05
	Chemical	MSP700-KOH	–	8.36	76.96	14.68	93.55	0.55	0.43	5.46	0.07	0.04
	N/A	WSP700	2.07	19.80	65.60	12.50	89.50	1.92	1.65	6.92	0.26	0.06
	Physical	WSP700–CO_2-800	–	21.00	79.00	–	81.10	0.60	1.50	16.8	0.09	0.16
		WSP700–CO_2-900	–	27.80	72.20	–	88.90	0.30	1.40	9.40	0.04	0.08
		WSP700–H_2O	–	32.6	67.40	–	97.86	0.59	1.54	0.01	0.07	0.00
	Chemical	WSP700–KOH	–	7.60	83.14	9.26	97.22	0.69	0.79	1.29	0.09	0.01

[a] O content was calculated by difference.

analysis showed that both physical and chemical activations caused a slight increase in the total carbon content, which can positively affect electrochemical performance since carbon is the most electrically conductive part of biochar used as an electrode material for supercapacitors [31]. It can also be seen that hydrogen content decreased from 1.79 to 2.25 wt% to 0.30–1.10 wt% (corresponding to H/C of 0.04–0.11) due to the dehydration during high-temperature activation. The decrease in H/C also indicate a higher stability and carbon sequestration potential of biochar [32]. On the other hand, the O/C ratio remains almost the same for both pristine and activated biochar, indicating that activation did not greatly affect its polarity. However, all O/C ratios (0.00–0.06) were significantly lower than the EBC standard limit (<0.4) for stable biochar [33].

3.1.2. Specific surface area

Porosity and pore-size distribution are important for enhancing capacitive performance by providing active ion sites. Extensive studies have found that there is a positive relationship between Brunauer–Emmett–Teller (BET) surface area and EDLC of biochar materials [31,34]. The nitrogen and CO_2 adsorption-desorption isotherms are shown in Figs. S1 and S2. The BET surface area was calculated from N_2 physical adsorption–desorption analysis performed on the biochars. The results showed that activated biochars exhibit higher specific surface areas (451–1061 $m^2\ g^{-1}$) compared to untreated biochars (up to 30 $m^2\ g^{-1}$), proving that physical and chemical activation are both effective methods to increase specific surface area of biochar.

The specific surface area (S_{BET}) and pore-size distribution of biochar are important parameters that affect ion diffusion, charge transport, capacitance, and electrical conductivity [12,35]. According to Table S1, activation processes can significantly increase the S_{BET} of biochar, with higher specific surface areas recorded here for activated biochar obtained from chemical activation ($S_{BET\ KOH} > S_{BET\ CO2} \approx S_{BET\ H2O}$). In this study, physically activated SWP, OSR, MSP, WSP, and OAK biochar presented 451–661, 461–530, 451–610, 482–548, and 619–730 $m^2\ g^{-1}$, respectively, while KOH chemical activation exhibited a relatively higher specific S_{BET} of 1061, 800, 739, 851, and 854 $m^2\ g^{-1}$, respectively. This is in line with findings from literature where chemical activation has shown to have a greater impact on pore formation in biochar than physical activation [36]. During KOH activation, a large number of inner channels in the biochar are generated, resulting in a high specific surface area. This could be because carbon in the reduction state can selectively react with high-energy K^+ ions in the oxidation state during a redox reaction, release H_2, and can further increase the pore area [30].

On the other hand, the BET results indicate that WBs has a higher S_{BET} (up to 1061 $m^2\ g^{-1}$) compared to SBs (up to 851 $m^2\ g^{-1}$). According to the proximate analysis and BET results, low-ash biochars have higher specific surface areas than high-ash biochars, probably because ash particles tend to fill in the pores of biochar, reducing the available surface area for N_2 and CO_2 adsorption [28]. During the pyrolysis process of biomass, the inorganic elements (e.g. calcium, potassium, and magnesium) remain in the biochar as ash content [24]. These minerals can fill in the micropores and mesopores of biochar, reducing the overall porosity and available surface area. High-ash biochar may also have a more compact structure with fewer and larger pores, further reducing the available surface area [37]. Therefore, biochar with a low ash content typically has a more open and porous structure, with smaller pores and a higher specific surface area, making it more suitable for various applications, such as gas adsorption and water treatment.

From the PSD figures (Fig. 1a, b, c, d) it can be seen that the physically activated biochars present a bimodal pore size distribution, with narrow micropores centred at 0.5–0.6 nm and broader small mesopores centred at 3.5–4 nm. In case of KOH activated sample, it presents a trimodal PSD, with micropores centred at 0.5–0.6 and 1 nm and same mesopores range, which provides addition evidence that chemical activation preferentially generates micropores. The chemically activated biochars produced more micropores compared to physically activated ones, which can be attributed to the different mechanisms of pore formation. These micropores are created by the reaction of the chemical agent with the carbonaceous material, leading to the removal of small fragments of carbon, and the formation of small cavities within the biochar [38]. In contrast, physical activation creates pores by the removal of volatile matter and by the reaction of C with CO_2 or H_2O, which leads also to the formation of micropores and mesopores,

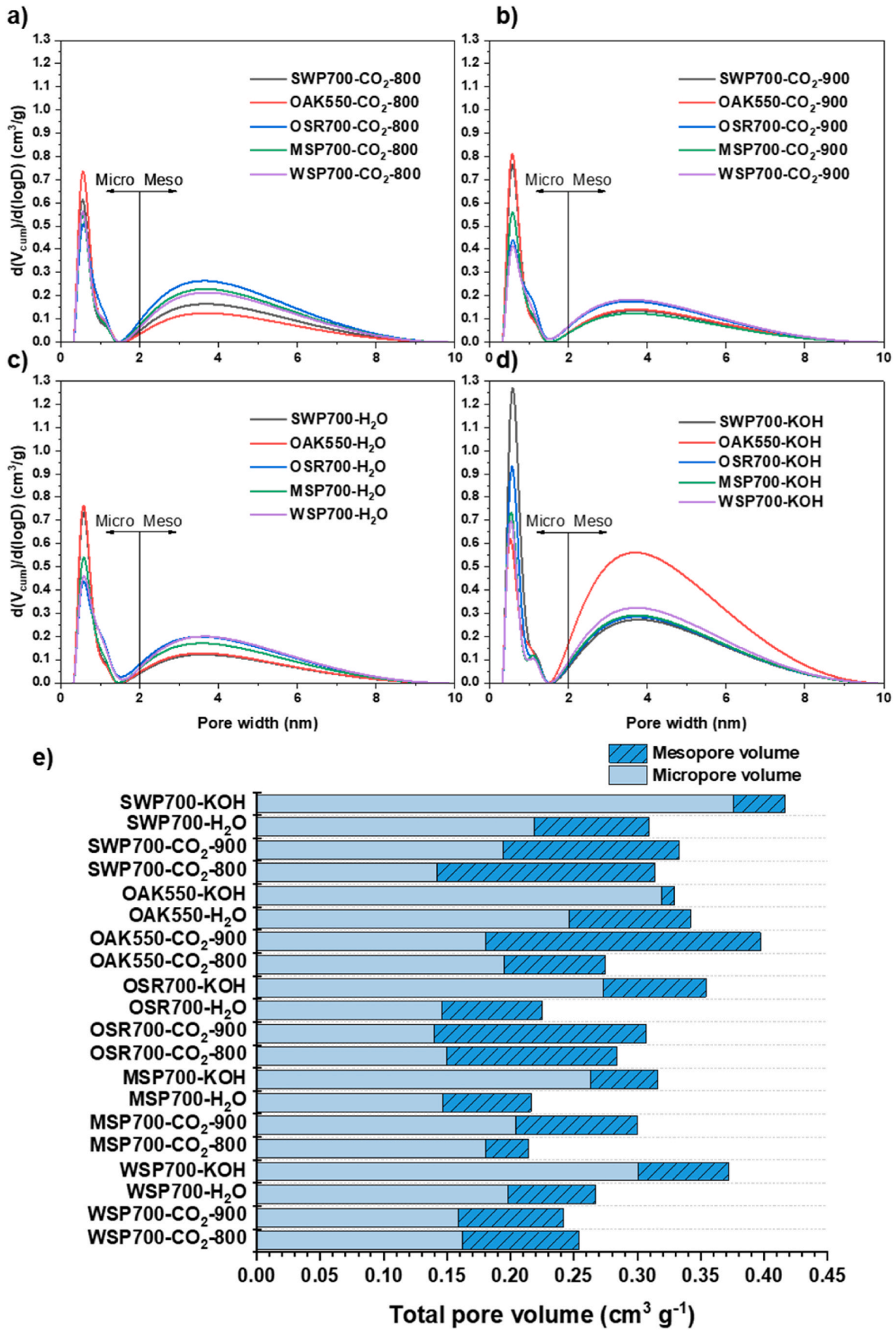

Fig. 1. Pore size distribution of activated biochars with a) CO_2 activation at 800 °C, b) CO_2 activation at 900 °C, c) steam activation, and d) KOH activation. e) Total pore volume and distribution of micro/mesopores of activated biochars.

however, not to the extent of chemical activation [39].

To gain further insight into the pores of the biochar material, we analysed the pore size distribution. Fig. 1e show that the total pore volume resulting from KOH activation is higher than that from physical activation, which agrees with the specific surface area results. Interestingly, chemical activation showed a stronger impact on pore distribution of SBs than WBs, i.e. SB exhibited a higher average pore diameter than WB by about 12.2%, possibly due to the ash etching [30]. This effect would possibly play a key role in the electrochemical performance, as electrolyte ions tend to occupy mesopores (2–50 nm) rather than micropores (<2 nm) [34]. Therefore, SB with chemical activation could be a more suitable candidate regarding the electrochemical application than SB with physical activation due to higher mesopore distribution.

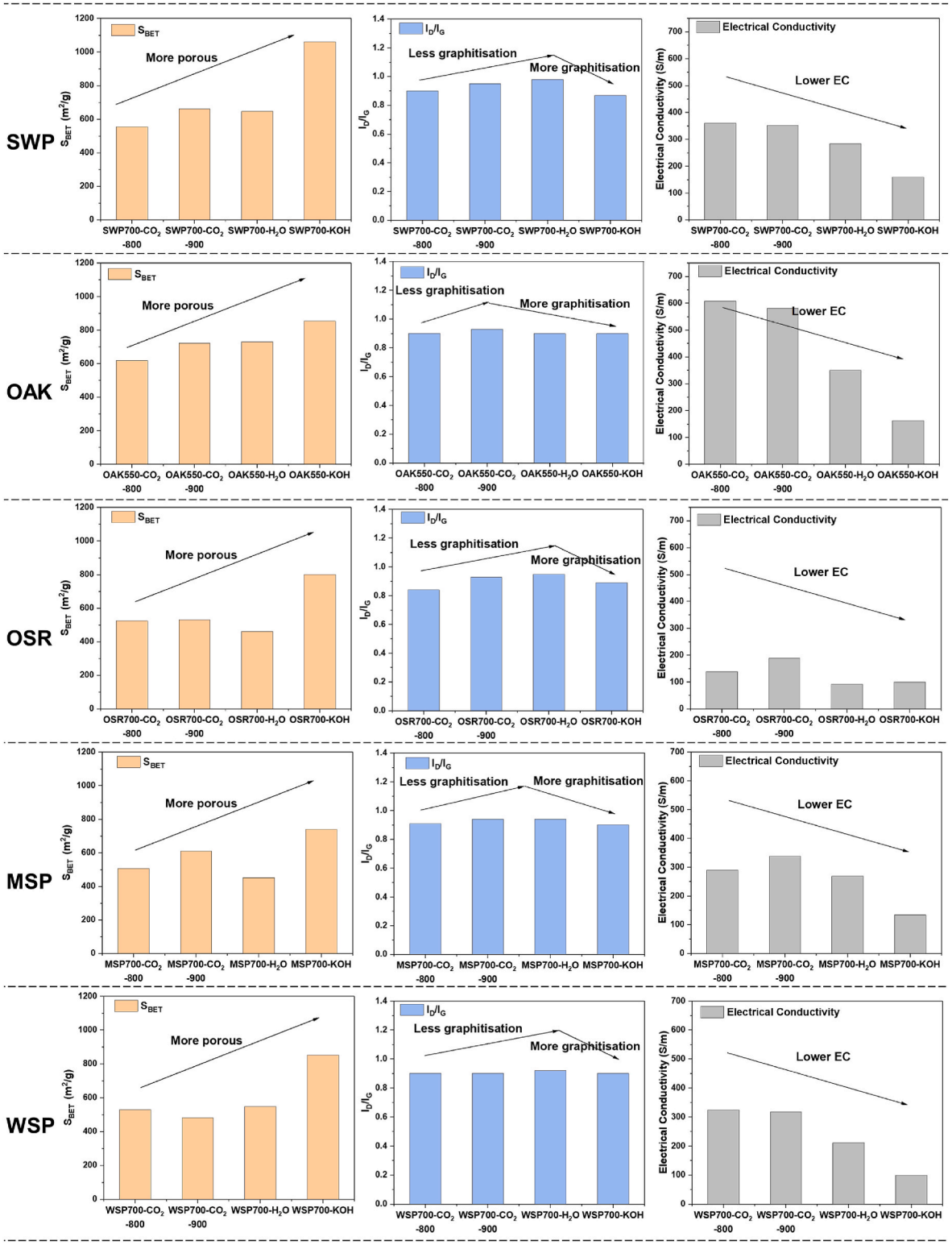

Fig. 2. Comparison of trends for S_{BET}, graphitisation degree, and electrical conductivity activated biochars.

3.1.3. Electrical conductivity and degree of graphitisation

As previously indicated, a great number of publications stated that enhanced electrical conductivity (EC) of activated carbons can result in improved electrochemical performance [5,9]. Generally, the EC results (Fig. 2, Table S1) in this study indicate that physical activation leads to higher values compared to chemical activation. This is likely due to the formation of a more substantial solid carbon-based structure during physical activation, i.e., high FC, which provides more pathways for electron transfer and ion diffusion [34]. In contrast, chemical activation produced a larger quantity of VM, which is mostly composed of organic compounds that are not electrically conductive. Interestingly, chemically activated biochar generally had high S_{BET} but low EC, which may due to an enhanced resistance effect due to longer charge transfer routes [34]. Physical activation methods produced biochars with moderate S_{BET} (451–730 m^2/g), rich micropores, and high EC (90–608 S/m) (Table S1). This is because these methods involve heating the biochar in the presence of CO_2 or steam, which can result in the removal of volatile compounds and the creation of micropores in the biochar structure [39]. These micropores can provide a moderate SSA for electrochemical reactions by providing pathways for electron transfer and ion diffusion to some extent. On the other hand, KOH activation methods produced biochars with a higher S_{BET} (739–1061 m^2/g) and a great amount of micropores and mesopores, but with a relatively negative impact on EC performance (99–159 S/m). This may be because KOH activation involves using a chemical agent that can create mesopores in the biochar structure [17]. While the mesopores can enhance the biochar's S_{BET}, they can also decrease the biochar's EC by increasing gaps between carbon matrix [34]. However, the relationship between S_{BET} and structure of carbon matrix needs to be confirmed.

Therefore, to gain further insights into the effect of different activation modes on the structure of the carbon matrix in the activated biochar, we used Raman spectroscopy. The D band (disorder carbon peak) and G band (aromatic carbon peak) are two distinctive peaks observed at 1350 and 1590 cm^{-1}, respectively. The degree of graphitisation (I_D/I_G) and the distribution and state of sp2 bonds are critical factors affecting the conductivity of carbon-based electrodes [40]. The results in Fig. S3 and Table S2 show that both G band and D band peaks were present in all activated biochar samples, and had a similar I_D/I_G ratio (ranging from 0.84 to 1.02) regardless of the feedstock used. This suggests that the dominant factor affecting the ratio of defective carbon to aromatic organisation was the thermal treatment temperature (700–900 °C) and activation methods, rather than the feedstock type [40]. Physical and chemical activation can both reduce the intensity of I_D and I_G peaks, but the extent of this reduction depends on the activation method. The I_D/I_G values of the representative MSP activated biochar (Fig. S4a) followed the trend $I_D/I_{gH2O} \approx I_D/I_{gCO2\ 900} > I_D/I_{gCO2\ 800} > I_D/I_{gKOH}$, indicating that physical activation resulted in a higher content of disordered carbon, while KOH activation led to higher amounts of aromatic organisation. Despite the low degree of graphitisation of physically activated biochar, its EC is high. This result was different from the common sense that a positive correlation between carbon material's graphitisation degree and EC exists. This is because the EC of carbon materials is not only influenced by their graphitisation degree but also by their SSA and porosity [17]. In this case, SSA emerges as the primary factor influencing EC.

In the present study, chemically activated biochar, despite having an aromatic carbon structure and high S_{BET}, can exhibit lower electrical conductivity due to its high surface area and non-conductive VM content. This phenomenon seemed similar in WBs and SBs. Importantly, the trends reveal that EC decreases as the SSA of biochar samples increases, as expected. However, it is noteworthy that biochars with a higher degree of graphitisation still exhibit lower EC (Fig. 2). This implies that the production of more ordered aromatic carbon in biochar does not consistently lead to higher EC but is often associated with higher electrical resistance, attributable to the gaps between carbon matrices (high SSA).

When the activation temperature for CO_2 increased from 800 to 900 °C, a slight increase in the I_D/I_G ratio was observed in all biochars, suggesting that the higher CO_2 activation temperature resulted in more disordered carbon layers. This is likely due to increased gasification of carbon and formation of defects within the carbon planes, resulting in a reduction in the degree of graphitisation [41]. In summary, the implementation of physical and chemical activation techniques can serve as effective methods for enhancing the carbon skeleton structure of biochar and thereby improving its EC. However, it should be noted that the presence of significantly high SSA (>730 m^2/g) and non-conductive VM can limit the influence of the graphitisation structure on EC. Thus, it is important to identify biochar properties that influence its electrochemical performance the most, i.e., SSA, in this case.

3.1.4. Functional groups

FTIR spectroscopy was used to identify the remaining superficial functional groups on biochar before and after activation. Fig. S4b shows the FTIR pattern of the MSP group of samples. According to previous studies, the absorption peaks at ~2916 cm^{-1} are attributed to saturated C–H stretching vibration (aliphatic C–H) and a wide peak at around 3200-3500 cm^{-1} is related to –OH stretching, both of which are typically observed in biochar materials in high-wavelength regions [40]. However, in the high-temperature pyrolysed biochars and activated biochars analysed in this study, these peaks are not clearly observed, likely due to the dehydration of cellulosic and ligneous components that occurs at 350–500 °C [40]. The peaks at 1340-1465 cm^{-1} are related to the bending vibration of aromatic C–C. The intensity of C═O, aromatic C═C, and O–C–O (carboxylate) stretching at around 1593-1700 cm^{-1} was found to be strong, especially for chemically activated samples, which might contribute to the pseudocapacitive performance of the biochar materials [13,30,42]. The band of out-of-plane bending for CO_3^{2-} was observed after physical and chemical activations which is contributed by $CaCO_3$ in ash content, and thereby were found to be more prevalent in the SBs as opposed to the WBs. Furthermore, the influence of activation temperature on the intensity of these vibrations was found to be relatively insignificant. Additionally, SBs (OSR, MSP, and WSP) exhibited a medium peak at ~1240 cm^{-1}, attributed to C–O stretching of carboxylic, ester, and ether groups, which were not observed in activated woody biomass-derived SWP and OAK biochars. The intensity of C–O stretching peaks can be augmented to some extent through the utilisation of elevated physical activation temperatures. This phenomenon arises as a consequence of the thermal stability of these C–O stretching bonds, which persist even after the gasification of the carbon skeleton at temperatures as high as 900 °C.

In summary, apart from the high-thermally-stable C–O peak at ~1240 cm^{-1}, the impact of KOH activation on biochars, especially the generation of carbonyl groups, is more significant than that of physical activation. This is evidenced by the strong peaks observed at 1600−1800 cm-1, which are related to carbonyl groups [43]. The presence of carbonyl groups on the surface of biochar can enhance its ability to adsorb and desorb ions, which can lead to the formation of reactive oxygen species and thereby can be beneficial for electrochemical applications [44]. These results are consistent with the proximate analysis results. Specific relationship between biochar's FTIR results and its electrochemical properties will depend on the type and quantity of functional groups present on the biochar's surface, which will be discussed in the next section.

3.2. Electrochemical performances of activated biochar

3.2.1. Cyclic voltammetry (CV) measurement

The potential application of activated biochar produced from woody and straw biomass as a working electrode material in supercapacitors was explored. In Fig. 3a, b, c, and d, all activated biochars were compared at a scan rate of 80 mV s^{-1}. The potential of raw biochar ranged from −1 to 0 V in a quasi-reversible electron transfer process.

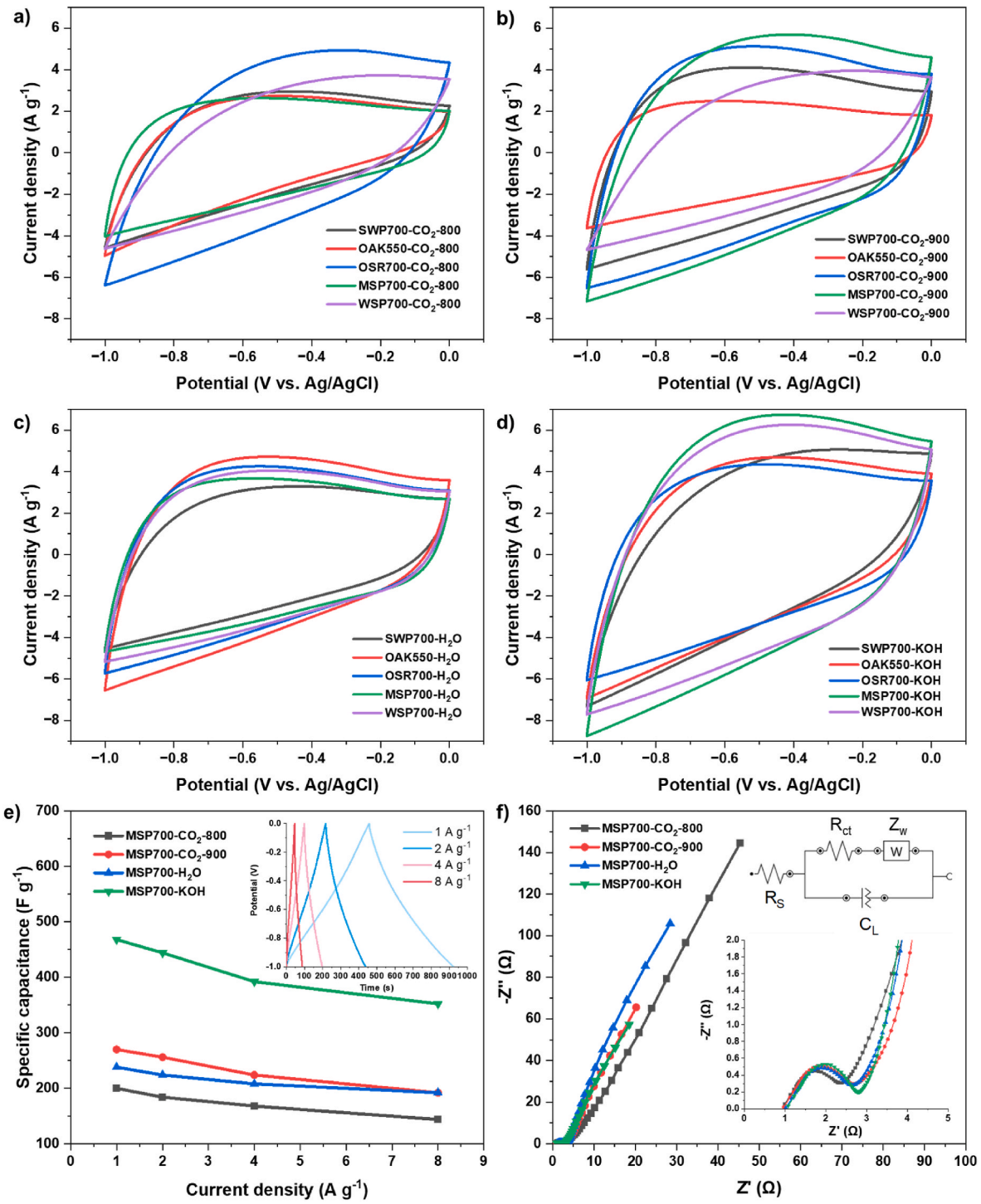

Fig. 3. Cyclic voltammetry curves of MSP700 activated biochars with a) CO_2 activation at 800 °C, b) CO_2 activation at 900 °C, c) steam activation, and d) KOH activation. e) Capacitance of representative MSP activated biochars. f) Electrochemical impedance spectroscopy of representative MSP activated biochars.

The CV results of all activated biochars showed good symmetry and semi-rectangular shapes, indicating the formation of electric double-layer capacitance (EDLCs). Increasing the scan rate from 10 to 80 mV s^{-1} led to an increase in the current range of the CV profile without distorting the rectangle, highlighting the good capacitive properties of the activated biochar.

The shapes of the CVs varied depending on the feedstock and activation method. Specifically, the chemically activated samples using KOH (Fig. 3d) exhibited the best capacitive performance with the largest integral area of curves. This can be attributed to the higher S_{BET} generated by KOH activation compared to physical activation methods and a more prominent presence of surface functional groups (carbonyl groups) as seen through the FTIR spectra. This also suggests that the surface area and surface functionality play a more prominent role than the EC of biochar in determining the capacitive properties of biochar. Additionally, SBs such as MSP, WSP, and OSR generally showed higher CV capacitance than WBs such as SWP and OAK (Fig. 3b), which also can be explained by their higher S_{BET} and an ash content, which may have more electroactive elements such as Fe, Mn etc. Compared to wood [45]. Indepth investigation of the role of metals in the ash was out of the scope

of this study and will be investigated in the future work.

3.2.2. Charge/discharge measurements (GCD) measurement

Fig. 3e shows galvanostatic charge/discharge (GCD) curves for the representative MSP activated biochar over a range of current densities from 1, 2, 4, and 8 A g^{-1}. When tested at a current density of 1 A g^{-1}, the activated biochars demonstrated discharge times ranging from 138 s (SWP700–CO_2-800) to 468 s (MSP700-KOH). In comparison to the raw biochars, all activated biochars exhibited superior capacitive performance. In addition, it can be seen that the IR drops are generally negligible, implying that the activated biochars have good conductivities which agreed with the EC results (Table S1). The specific capacitance is a representative indicator of electrochemical performance showing the ratio of the electric charge stored on biochar particle to the electric potential difference. Fig. 4 displays the summary specific capacitance results for biochars produced from different feedstocks and activation methods. The maximum specific capacitance value was observed at the current density of 1 A g^{-1}, which were 374 (SWP700–KOH), 406 (OSR700-KOH), 468 (MSP700-KOH), 378 (WSP700–KOH), and 330 (OAK550-KOH) F g^{-1}, respectively. Generally, activated biochar, produced via chemical activation showed higher capacitances compared to those activated through physical activation treatments. This also reiterates the earlier findings that an optimum combination of specific surface area, suitable pore-size distribution and surface functionalities (carbonyl groups) may have a more prominent role in deciding the specific capacitance. Surprisingly, WBs, with their higher EC, higher S_{BET} and lower ash content than SB, have a slightly lower specific capacitance (Fig. 4). One possible explanation could be that the presence of electroactive materials such as Fe/Mn oxides found more abundantly in SB contributes to pseudocapacitance during charging and discharging as indicated by proximate analysis results.

The power densities of activated biochars have been further determined and compared with their energy densities shown in the Ragone plot in Fig. S5. The results show, that the MSP biochars have considerably higher power densities and energy densities than conventional biochars, especially, MSP700-KOH reached 65.0 Wh kg^{-1} at the power density of 500 W kg^{-1}, which is promising even compared to other laboratory-synthesised activated biochars (Table S3). The most significant contributing factors are its high specific surface area, surface functionalities and a favourable pore-size distribution (mesopore volume).

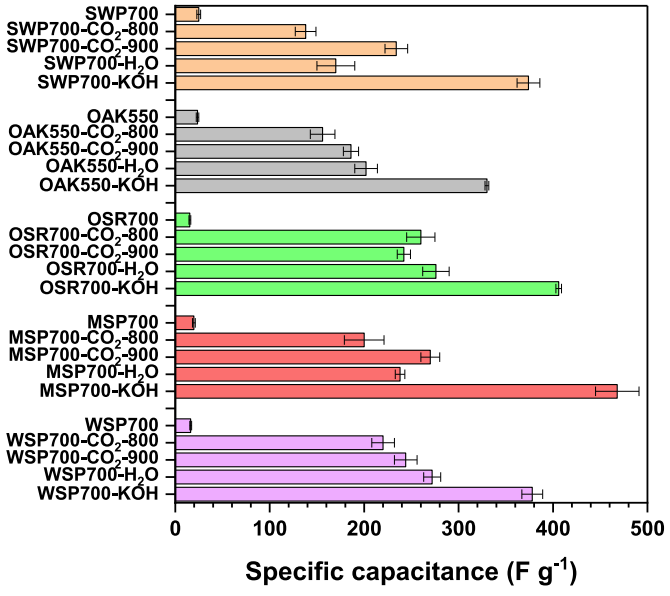

Fig. 4. Specific capacitances of SWP, OAK, OSR, MSP, and WSP raw and activated biochars.

3.2.3. Electrochemical impedance spectroscopy (EIS) measurement

Further investigation into the activated biochars was conducted through the utilisation of electrochemical impedance spectroscopy (EIS) measurements which enabled the evaluation of ion transport processes. Fig. 3e shows the Nyquist plots of activated MSP biochars. All Nyquist curves exhibit a semicircle in the high frequency region representing the impedance of faradaic reactions, while a straight line represents a typical capacitive performance of synthesised electrode. According to previous studies, a smaller-size semicircle indicates a faster ions transfer rate with low charge-transfer resistance, while a larger slope of straight line implies better capacitive properties [46]. A bulk solution resistance (R_s) and a charge transfer resistance (R_t) can be extracted from the semicircle intersection with the abscissa in Nyquist plots. The Rs of all activated biochars were measured to be around 1.01–1.05 Ω which are contributed by the consistent electrolyte used in this project, namely 4 M KOH. The R_{ct}, also called Faraday resistance, was found to have a negative impact on the specific power of the supercapacitor, thus, MSP700-KOH with the lowest R_{ct} (1.85 Ω) among all seems to be the best candidate for being biochar supercapacitor electrode regarding the fastest ions transfer rate. An additional line of evidence supporting the superior electrochemical performance of chemically activated biochars is their lower charge transfer resistance (R_{ct}). Furthermore, the present study has revealed that biochars derived from SBs possess lower R_{ct} than those derived from WBs, a finding that is consistent with the characterisation results.

The effects of differences in biomass types and activation methods on the biochar impedances can also be distinguished in Nyquist plots. MSP700-KOH, as the sample with the highest capacitance, possessed the least extensive Warburg region (the straight line at low-frequency) showing the shortest ion diffusion channel lengths and the lowest barrier of ion movement among all activation methods, generally following a Warburg impedance order of KOH < CO_2-900 < H_2O < CO_2-800. The KOH activated MSP ranked first owing to its highest surface area and desirable mesopore percentage, which provide excellent ion diffusion routes. In addition, from an EIS point of view, straw biochar is more favourable due to the electrical-conductive ash content. However, the relationship between ash composition and biochar impedance is complex and requires further study. For example, metal oxides, such as Fe_2O_3 and MnO_2 can provide biochar active site for pseudocapacitive performance and also reduce the electrochemical impedance. Therefore, detailed characterisation of the ash composition and its distribution in the biochar should be conducted in future studies.

3.3. Current status and future opportunities

To evaluate the decisive factors affecting the specific capacitance of activated biochar, a Pearson correlation coefficient analysis was conducted (Fig. 5). The Pearson correlation coefficient analysis assessed the relationship between specific capacitance and various properties of activated biochar, providing insights into the key factors influencing electrochemical performance. Based on the results, the specific capacitances of the different activated biochars were positively correlated with VM (0.87) ($p < 0.001$). This confirmed that the VM content or pseudocapacitance played a key role in determining the electrochemical specific capacitance of the activated biochar (Pearson correlation coefficient of 0.55, $p < 0.05$), however, this is based on the materials with sufficient SSA. It is evident by the negligible capacitance (<40 F/g) of raw biochars with low SSA (<90 m^2/g) and high VM (>9.9 wt%). Therefore, where the SSA of the biochar is sufficiently large (>450 m^2/g), turning to consideration of increased pseudo-capacitance or selective addition of specific functional groups may be a more effective approach than merely focusing on increasing SSA of biochar material (corresponding to EDLC). Contrary to the prevailing belief in many studies [47–49] that high EC of biochar materials leads to increased volumetric power and energy densities as electrode materials in supercapacitors, this study observed a negative correlation between specific capacitances

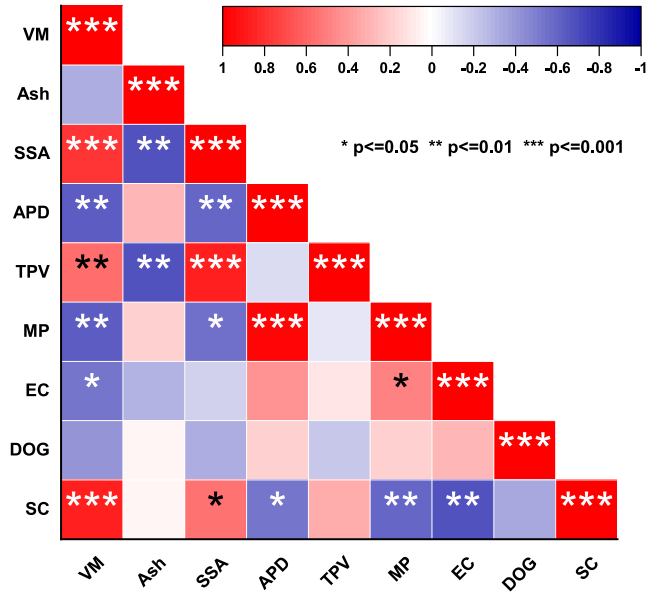

Fig. 5. Pearson correlation coefficient matrices for relationship between physicochemical properties and electrochemical performance of carbon materials, including volatile matter (VM) content, ash content, specific surface area (SSA), average pore volume (APV), total pore volume (TPV), mesopore percentage (MP), electrical conductivity (EC), and degree of graphitisation (DOG), and specific capacitance (SC).

and EC (−0.66, $p < 0.01$). The Pearson correlation matrix analysis confirmed that the high SSA and EDLC resulting from the activation methods outlined in this work indirectly raise the transport distance of ions within the biochar material. Consequently, this increase in distance enhances resistance, ultimately reducing the EC. Therefore, in practical terms, the findings suggest that a high EC of biochar material alone does not necessarily increase the capacitance of the material. This is because achieving a high EC may come at the expense of other crucial properties, such as functionality and SSA. The interplay of these factors needs to be carefully considered in the design and application of biochar materials in supercapacitors. To further enhance the specific capacitance, it is necessary to upgrade the EDLC while maximising the EC, or to find a method that has different principle from physical-chemical activation but achieves both properties at the same time. Based on the results, it is evident that the relationship between the physicochemical characteristics of biochar and its electrochemical performance is intricate. This investigation suggests that surface area, pore distribution, surface functionalities, and ash content are more significant contributors to the electrochemical performance of biochar than EC. Nonetheless, it cannot be completely ruled out that there exists a threshold value of EC beyond which other factors become more influential. This needs further investigation in the future.

In this study, activated biochars produced via physical and chemical activation of woody and straw biomass are characterised systematically for their physico-chemical and electrochemical properties. Table S3 shows that the obtained specific capacitance and energy density of MSP700-KOH is higher than previous reported biochars produced under similar conditions. Additionally, the cost of straw biomass (147–156 £/ton) and chemical activation (0.05–0.06 £/g carbon production) are substantially lower than that of woody biomass and physical activation (Table S4). Considering the generally low activation temperature (700 °C) employed and short activation time (60 min), MSP700-KOH seems to be a promising and a suitable option for supercapacitors' electrodes. Furthermore, the thorough electrochemical analysis sheds light on the crucial parameters that contribute to the electroactivity of biochars. This comprehension can aid in utilising electroactive biochar in various applications, including but not limited to electrochemical energy storage, electrochemical energy conversion (such as electrocatalysis and fuel cells), and Microbial Electrochemical Technology (MET) like microbial fuel cells, among others [45,50]. More research into improving and optimising the electrochemical properties of biochar can be explored by the production of biochar and biochar-composites, such as using other electroactive materials (transition metal oxides, hetero-atom doping) along with biochar via other pre-post treatments such as co-pyrolysis of biomass with metal oxide precursors. On the other hand, future research should also incorporate full life cycle analysis and techno-economic analysis of the production and various electrochemical applications of electroactive biochar to understand the scope of sustainable scale-up of this technology.

4. Conclusion

This work comprehensively showed the extent to which the type of biomass (woody/straw biomass) and the activation method affect different biochar physicochemical properties and subsequently their electrochemical performance as potential supercapacitor electrode. The results revealed that straw biomass biochars with high-ash content (21.0–32.8 wt%) had higher specific capacitance than woody biochars, despite their lower electrical conductivity and surface area, probably due to the higher pseudocapacitance. Additionally, compared to physical activation, chemical activation using KOH was found to increase the volatile matter content and surface area of the biochar, resulting in improved electrochemical performance due to the increase of both double-layer and pseudocapacitive properties. Importantly, this study underscores that exclusively concentrating on enhancing electrical conductivity for biochar's electrochemical performance is not practical, as it can come at the expense of reduced porosity. These findings provide valuable insights needed for the development of sustainable and efficient electrode materials for electrochemical energy storage devices by choosing the optimal combination of feedstock types and activation methods.

CRediT authorship contribution statement

Jiacheng Sun: Writing – original draft, Validation, Software, Methodology, Investigation, Funding acquisition, Formal analysis, Data curation, Conceptualization. **Anjali Jayakumar:** Writing – review & editing, Writing – original draft, Visualization, Methodology, Investigation, Conceptualization. **Carlos G. Díaz-Maroto:** Investigation, Data curation. **Inés Moreno:** Writing – review & editing, Methodology. **Javier Fermoso:** Writing – review & editing, Supervision, Methodology, Investigation. **Ondřej Mašek:** Validation, Supervision, Resources, Project administration, Methodology, Funding acquisition, Conceptualization.

Declaration of competing interest

The authors declare that they have no known competing financial interests or personal relationships that could have appeared to influence the work reported in this paper.

Data availability

Data will be made available on request.

Acknowledgments

J. Sun acknowledge the UK Carbon Capture and Storage Research Centre (UKCCSRC) (EP/W002841/1) for the flexible fund 'An integrated strategy for long-term carbon sink and sustainable supercapacitor material production'. The UKCCSRC is supported by the Engineering and Physical Sciences Research Council (EPSRC), UK, as part of the UKRI

Energy Programme. J. Fermoso gratefully acknowledges the financial support from the Comunidad de Madrid through the Talent Attraction Programme (2018-T1/AMB-10023). We thank Dr Andrei Gromovii (School of Chemistry, University of Edinburgh) for assistance in analytical work.

Appendix A. Supplementary data

Supplementary data to this article can be found online at https://doi.org/10.1016/j.biombioe.2024.107180.

References

[1] J. Sun, O. Norouzi, O. Mašek, A state-of-the-art review on algae pyrolysis for bioenergy and biochar production, Bioresour. Technol. (2021) 126258, https://doi.org/10.1016/j.biortech.2021.126258.
[2] IRENA, Renewable Power Generation Costs in 2021, 2022. Abu Dhabi.
[3] (IEA) International Energy Agency, (EPO) European Patent Office, Innovation in Batteries and Electricity Storage, Iea, 2020, pp. 1–98. https://www.iea.org/reports/innovation-in-batteries-and-electricity-storage.
[4] D. Zhang, C. Tan, W. Zhang, W. Pan, Q. Wang, L. Li, Molecules Expanded Graphite-Based Materials for Supercapacitors: A Review, 2022, https://doi.org/10.3390/molecules27030716.
[5] V. Hoffmann, C. Rodriguez Correa, D. Sautter, E. Maringolo, A. Kruse, Study of the Electrical Conductivity of Biobased Carbonaceous Powder Materials under Moderate Pressure for the Application as Electrode Materials in Energy Storage Technologies, 2018, https://doi.org/10.1111/gcbb.12545.
[6] M. Maher, S. Hassan, K. Shoueir, B. Yousif, M.E.A. Abo-Elsoud, Activated carbon electrode with promising specific capacitance based on potassium bromide redox additive electrolyte for supercapacitor application, J. Mater. Res. Technol. 11 (2021) 1232–1244, https://doi.org/10.1016/J.JMRT.2021.01.080.
[7] Q. Ke, J. Wang, Graphene-based materials for supercapacitor electrodes – a review, J. Mater. 2 (2016) 37–54, https://doi.org/10.1016/J.JMAT.2016.01.001.
[8] C. Zhi, Y. Huang, Y. Yao, J. Foroughi, Z. Lu, R. Raad, F. Safaei, J. Xi, Z. Liu, Carbon nanotube based fiber supercapacitor as wearable energy storage, wearable energy storage, Front. Mater. 6 (2019) 138, https://doi.org/10.3389/fmats.2019.00138.
[9] U. Fischer, R. Saliger, V. Bock, R. Petricevic, J. Fricke, Carbon Aerogels as Electrode Material in Supercapacitors, Kluwer Academic Publishers, 1997.
[10] M.H. Kim, I.T. Jeong, S.B. Park, J.W. Kim, Analysis of environmental impact of activated carbon production from wood waste, Environ. Eng. Res. 24 (2019) 117–126, https://doi.org/10.4491/eer.2018.104.
[11] Q. Li, X. Bai, Q. Meng, T. Chen, W. Zhu, W. Yao, J. Lei, L. Zhang, X. Yang, X. Wei, T. Duan, Porous biochar generated from natural Amorphophallus konjac for high performance supercapacitors, Appl. Surf. Sci. 448 (2018) 16–22, https://doi.org/10.1016/J.APSUSC.2018.04.086.
[12] R. Mehdi, A.H. Khoja, S.R. Naqvi, N. Gao, N.A.S. Amin, A review on production and surface modifications of biochar materials via biomass pyrolysis process for supercapacitor applications, Catalysts 12 (2022), https://doi.org/10.3390/catal12070798.
[13] S.E.M. Pourhosseini, O. Norouzi, H.R. Naderi, Study of micro/macro ordered porous carbon with olive-shaped structure derived from Cladophora glomerata macroalgae as efficient working electrodes of supercapacitors, Biomass Bioenergy 107 (2017) 287–298, https://doi.org/10.1016/J.BIOMBIOE.2017.10.025.
[14] J.K. Soeherman, A.J. Jones, P.J. Dauenhauer, Overcoming the entropy penalty of direct air capture for efficient gigatonne removal of carbon dioxide, ACS Eng. Au. 3 (2023), https://doi.org/10.1021/acsengineeringau.2c00043.
[15] J. Shaheen, Y.H. Fseha, B. Sizirici, Performance, life cycle assessment, and economic comparison between date palm waste biochar and activated carbon derived from woody biomass, Heliyon 8 (2022) e12388, https://doi.org/10.1016/J.HELIYON.2022.E12388.
[16] A.K. Sakhiya, A. Anand, P. Kaushal, Production, Activation, and Applications of Biochar in Recent Times, Springer Singapore, 2020, https://doi.org/10.1007/s42773-020-00047-1.
[17] I. Yang, M. Jung, M.S. Kim, D. Choi, J.C. Jung, Physical and chemical activation mechanisms of carbon materials based on the microdomain model, J. Mater. Chem. A 9 (2021) 9815–9825, https://doi.org/10.1039/d1ta00765c.
[18] Y. Zhang, Y.-P. Zhao, L.-L. Qiu, J. Xiao, F.-P. Wu, J.-P. Cao, Y.-H. Bai, F.-J. Liu, Insights into the KOH activation parameters in the preparation of corncob-based microporous carbon for high-performance supercapacitors, Diam. Relat. Mater. (2022) 109331, https://doi.org/10.1016/J.DIAMOND.2022.109331.
[19] B. Marinho, M. Ghislandi, E. Tkalya, C.E. Koning, G. de With, Electrical conductivity of compacts of graphene, multi-wall carbon nanotubes, carbon black, and graphite powder, Powder Technol. 221 (2012) 351–358, https://doi.org/10.1016/J.POWTEC.2012.01.024.
[20] C. Wurzer, O. Mašek, Feedstock doping using iron rich waste increases the pyrolysis gas yield and adsorption performance of magnetic biochar for emerging contaminants, Bioresour. Technol. 321 (2021) 124473, https://doi.org/10.1016/J.BIORTECH.2020.124473.
[21] Y.H. Liu, H.C. Hsi, K.C. Li, C.H. Hou, Electrodeposited manganese dioxide/activated carbon composite as a high-performance electrode material for capacitive deionization, ACS Sustain. Chem. Eng. 4 (2016) 4762–4770, https://doi.org/10.1021/acssuschemeng.6b00974.
[22] D. Rehrah, M.R. Reddy, J.M. Novak, R.R. Bansode, K.A. Schimmel, J. Yu, D. W. Watts, M. Ahmedna, Production and characterization of biochars from agricultural by-products for use in soil quality enhancement, J. Anal. Appl. Pyrolysis 108 (2014) 301–309, https://doi.org/10.1016/J.JAAP.2014.03.008.
[23] R. Goudarzi, G. Hashemi Motlagh, The effect of graphite intercalated compound particle size and exfoliation temperature on porosity and macromolecular diffusion in expanded graphite, Heliyon 5 (2019) e02595, https://doi.org/10.1016/J.HELIYON.2019.E02595.
[24] O. Mašek, W. Buss, A. Roy-Poirier, W. Lowe, C. Peters, P. Brownsort, D. Mignard, C. Pritchard, S. Sohi, Consistency of biochar properties over time and production scales: a characterisation of standard materials, J. Anal. Appl. Pyrolysis 132 (2018) 200–210, https://doi.org/10.1016/J.JAAP.2018.02.020.
[25] J. Sun, V. Benavente, S. Jansson, O. Mašek, Comparative characterisation and phytotoxicity assessment of biochar and hydrochar derived from municipal wastewater microalgae biomass, Bioresour. Technol. (2023) 129567, https://doi.org/10.1016/J.BIORTECH.2023.129567.
[26] C.G. Díaz-Maroto, B. Sáenz de Miera, L. Collado, J. Fermoso, O. Mašek, P. Pizarro, D.P. Serrano, I. Moreno, J. Fermoso, Removal of NO at low concentration from air in urban built environments by activated miscanthus biochar, J. Environ. Manag. 336 (2023) 117610, https://doi.org/10.1016/J.JENVMAN.2023.117610.
[27] C.G. Díaz-maroto, O. Masek, P. Pizarro, D.P. Serrano, I. Moreno, J. Fermoso, Removal of NO at low concentrations from polluted air in semi-closed environments by activated biochars from renewables feedstocks, J. Environ. Manag. 341 (2023), https://doi.org/10.1016/j.jenvman.2023.118031.
[28] M. Zhang, Y. Zhu, Y. Lyu, Y. Luo, T. Duan, W. Li, P. Li, Impact of deashing treatment on biochar physicochemical properties and sorption mechanisms of naphthalene and 1-naphthol, Environ. Technol. Innov. 24 (2021), https://doi.org/10.1016/j.eti.2021.101960.
[29] P. Konnerth, D. Jung, J.W. Straten, K. Raffelt, A. Kruse, Metal oxide-doped activated carbons from bakery waste and coffee grounds for application in supercapacitors, Mater. Sci. Energy Technol. 4 (2021) 69–80, https://doi.org/10.1016/J.MSET.2020.12.008.
[30] Y. Gao, R. Sun, A. Li, G. Ji, In-situ self-activation strategy toward highly porous biochar for supercapacitors: direct carbonization of marine algae, J. Electroanal. Chem. 882 (2021) 114986, https://doi.org/10.1016/j.jelechem.2021.114986.
[31] X. Li, J. Zhang, B. Liu, Z. Su, A critical review on the application and recent developments of post-modified biochar in supercapacitors, J. Clean. Prod. 310 (2021) 127428, https://doi.org/10.1016/J.JCLEPRO.2021.127428.
[32] I.B.I. Ibi, Standardized product definition and product testing guidelines for biochar that is used in soil, Int. Biochar Initiat. 23 (2015). http://www.biochar-international.org/sites/default/files/Guidelines_for_Biochar_That_Is_Used_in_Soil_Final.pdf.
[33] European Biochar Foundation (EBC), Guidelines for a sustainable production of biochar, Eur. Biochar Found. (2016) 1–22.
[34] Z. Bian, H. Wang, X. Zhao, Z. Ni, G. Zhao, C. Chen, G. Hu, S. Komarneni, Optimized mesopores enable enhanced capacitance of electrochemical capacitors using ultrahigh surface area carbon derived from waste feathers, J. Colloid Interface Sci. (2022), https://doi.org/10.1016/J.JCIS.2022.09.123.
[35] R.K. Gupta, M. Dubey, P. Kharel, Z. Gu, Q.H. Fan, Biochar activated by oxygen plasma for supercapacitors, J. Power Sources 274 (2015) 1300–1305, https://doi.org/10.1016/J.JPOWSOUR.2014.10.169.
[36] Z. Xu, M. He, X. Xu, X. Cao, D.C.W. Tsang, Impacts of different activation processes on the carbon stability of biochar for oxidation resistance, Bioresour. Technol. 338 (2021) 125555, https://doi.org/10.1016/j.biortech.2021.125555.
[37] M. Marmiroli, U. Bonas, D. Imperiale, G. Lencioni, F. Mussi, N. Marmiroli, E. Maestri, Structural and functional features of chars from different biomasses as potential plant amendments, Front. Plant Sci. 9 (2018), https://doi.org/10.3389/fpls.2018.01119.
[38] A. Pathy, P. Pokharel, X. Chen, P. Balasubramanian, S.X. Chang, Activation methods increase biochar's potential for heavy-metal adsorption and environmental remediation: a global meta-analysis, Sci. Total Environ. 865 (2023) 161252, https://doi.org/10.1016/J.SCITOTENV.2022.161252.
[39] A. Colomba, F. Berruti, C. Briens, Model for the physical activation of biochar to activated carbon, J. Anal. Appl. Pyrolysis 168 (2022) 105769, https://doi.org/10.1016/J.JAAP.2022.105769.
[40] L. Zhao, X. Cao, O. Mašek, A. Zimmerman, Heterogeneity of biochar properties as a function of feedstock sources and production temperatures, J. Hazard Mater. 256–257 (2013) 1–9, https://doi.org/10.1016/J.JHAZMAT.2013.04.015.
[41] C. Jiang, G.A. Yakaboylu, T. Yumak, J.W. Zondlo, E.M. Sabolsky, J. Wang, Activated carbons prepared by indirect and direct CO2 activation of lignocellulosic biomass for supercapacitor electrodes, Renew. Energy 155 (2020) 38–52, https://doi.org/10.1016/J.RENENE.2020.03.111.
[42] J. Zeng, L. Wei, X. Guo, Bio-inspired high-performance solid-state supercapacitors with the electrolyte, separator, binder and electrodes entirely from: kelp, J. Mater. Chem. A 5 (2017) 25282–25292, https://doi.org/10.1039/c7ta08095f.
[43] S.E.M. Pourhosseini, O. Norouzi, P. Salimi, H.R. Naderi, Synthesis of a novel interconnected 3D pore network algal biochar constituting iron nanoparticles derived from a harmful marine biomass as high-performance asymmetric supercapacitor electrodes, ACS Sustain. Chem. Eng. 6 (2018) 4746–4758, https://doi.org/10.1021/acssuschemeng.7b03871.
[44] Y. Zhang, X. Xu, P. Zhang, Ling Zhao, H. Qiu, X. Cao, Pyrolysis-temperature depended quinone and carbonyl groups as the electron accepting sites in barley grass derived biochar, Chemosphere 232 (2019) 273–280, https://doi.org/10.1016/J.CHEMOSPHERE.2019.05.225.
[45] S. Joseph, O. Husson, E.R. Graber, L. Van Zwieten, S. Taherymoosavi, T. Thomas, S. Nielsen, J. Ye, G. Pan, C. Chia, P. Munroe, J. Allen, Y. Lin, X. Fan, S. Donne, The

electrochemical properties of biochars and how they affect soil redox properties and processes, Agronomy 5 (2015), https://doi.org/10.3390/agronomy5030322.
[46] M. Ren, Z. Jia, Z. Tian, D. Lopez, J. Cai, M.M. Titirici, A.B. Jorge, High performance N-doped carbon electrodes obtained via hydrothermal carbonization of macroalgae for supercapacitor applications, Chemelectrochem 5 (2018) 2686–2693, https://doi.org/10.1002/celc.201800603.
[47] R. Gabhi, L. Basile, D.W. Kirk, M. Giorcelli, A. Tagliaferro, C.Q. Jia, Electrical conductivity of wood biochar monoliths and its dependence on pyrolysis temperature, Biochar 2 (2020), https://doi.org/10.1007/s42773-020-00056-0.
[48] C. Zhao, Y. Shi, J. Xie, F. Lei, L. Zhang, Direct measurement of electrical conductivity of porous biochar monolith for supercapacitors, Mater. Res. Express 6 (2019), https://doi.org/10.1088/2053-1591/ab326e.
[49] V. Hoffmann, D. Jung, J. Zimmermann, C.R. Correa, A. Elleuch, K. Halouani, A. Kruse, Conductive carbon materials from the hydrothermal carbonization of vineyard residues for the application in electrochemical double-layer capacitors (EDLCs) and direct carbon fuel cells (DCFCs), Materials 12 (2019), https://doi.org/10.3390/MA12101703.
[50] T. Huggins, H. Wang, J. Kearns, P. Jenkins, Z.J. Ren, Biochar as a sustainable electrode material for electricity production in microbial fuel cells, Bioresour. Technol. 157 (2014) 114–119, https://doi.org/10.1016/J.BIORTECH.2014.01.058.